



OPEN ACCESS

EDITED BY

Adriano Martimbianco De Assis,
Catholic University of Pelotas, Brazil

REVIEWED BY

Qiwen Liao,
The Chinese University of Hong Kong, China
Marcos Roberto De Oliveira,
Federal University of Rio Grande do Sul, Brazil

*CORRESPONDENCE

Yu Zhang
✉ gz_zhangyu1980cmu@126.com
Chusong Zhou
✉ mdzcs28@163.com

[†]These authors have contributed equally to this work

RECEIVED 28 November 2024

ACCEPTED 27 February 2025

PUBLISHED 17 March 2025

CITATION

Zhu J, Wang S, Zhang Y and Zhou C (2025) Identification and validation of biomarkers associated with mitochondrial dysfunction and ferroptosis in rat spinal cord injury. *Front. Neurol.* 16:1526966. doi: 10.3389/fneur.2025.1526966

COPYRIGHT

© 2025 Zhu, Wang, Zhang and Zhou. This is an open-access article distributed under the terms of the [Creative Commons Attribution License \(CC BY\)](https://creativecommons.org/licenses/by/4.0/). The use, distribution or reproduction in other forums is permitted, provided the original author(s) and the copyright owner(s) are credited and that the original publication in this journal is cited, in accordance with accepted academic practice. No use, distribution or reproduction is permitted which does not comply with these terms.

Identification and validation of biomarkers associated with mitochondrial dysfunction and ferroptosis in rat spinal cord injury

Jingliang Zhu^{1†}, Shuai Wang^{1†}, Yu Zhang^{2*} and Chusong Zhou^{1*}

¹Department of Orthopaedics, Zhujiang Hospital, Southern Medical University, Guangzhou, China,

²Department of Orthopaedics, General Hospital of Southern Theatre Command of PLA, Guangzhou, China

Introduction: Mitochondrial dysfunction and ferroptosis have been implicated in the pathophysiological processes following spinal cord injury (SCI), with evidence suggesting their interplay influences neuronal cell survival and repair mechanisms. This study seeks to identify mitochondria- and ferroptosis-related biomarkers through comprehensive bioinformatics analysis.

Methods: Mitochondria- and ferroptosis-associated differentially expressed genes (DEGs) were identified through the integration of differential expression analysis and weighted gene co-expression network analysis. Two machine learning algorithms, least absolute shrinkage and selection operator (LASSO) and Boruta, were employed to isolate SCI-associated feature genes. Biomarkers were subsequently identified by analyzing their expression levels. An artificial neural network (ANN) diagnostic model was constructed to predict SCI likelihood based on these biomarkers. Further evaluations were performed using enrichment analysis, immune infiltration profiling, molecular modulation assessment, and drug prediction. The biomarkers' expression levels were validated using RT-qPCR.

Results: In this study, two biomarkers, Hcrt and Cdca2, linked to mitochondrial function and ferroptosis in SCI, were found to be highly expressed in SCI samples. Tissue-specific analysis from the GTEx database revealed expression of these biomarkers in brain and spinal cord tissues. The ANN model, constructed using these biomarkers, accurately discriminated between SCI and control samples. Enrichment analysis highlighted several co-enriched pathways for Hcrt and Cdca2, including "ubiquitin-mediated proteolysis," "endocytosis," and the "neurotrophin signaling pathway." Immune infiltration analysis, based on the Wilcoxon test, demonstrated significant differences in T follicular helper cell levels, which were lower in SCI samples compared to controls. Notably, T follicular helper cells exhibited a positive correlation with Hcrt and a negative correlation with Cdca2. Furthermore, seven transcription factors, including CEBPB, FOXO1, and GATA2, were identified as potential co-regulators of Hcrt and Cdca2. Drug prediction analysis revealed stable interactions of Cdca2 with pinosylvin, zinc acetate dihydrate, hydroquinone, lucanthone, and dasatinib. RT-qPCR validation confirmed the expression patterns of Hcrt and Cdca2 in alignment with the dataset, showing statistically significant differences.

Discussion: This study identifies Hcrt and Cdca2 as biomarkers related to mitochondrial function and ferroptosis in SCI, providing new insights for the diagnosis and mechanistic understanding of SCI.

KEYWORDS

spinal cord injury, ferroptosis, mitochondria, biomarker, machine learning

Introduction

Spinal cord injury (SCI) represents a significant central nervous system disorder, typically resulting from external mechanical forces that compromise both the structural integrity and function of the spinal cord. Such disruption hinders motor, sensory, and reflex functions below the level of the lesion (1). Annually, 250,000 to 500,000 individuals worldwide experience traumatic spinal cord injuries, with this incidence expected to rise due to increased transportation usage and an aging population (2). Current clinical management of SCI predominantly involves surgical and pharmacological approaches (3). While these strategies may alleviate some symptoms, they remain insufficient in restoring neurological function. Consequently, there is a critical need for novel therapeutic strategies to address this pressing medical challenge.

Mitochondria are double-membraned organelles that play a crucial role in various physiological functions such as adenosine triphosphate (ATP) synthesis, calcium ion homeostasis, apoptosis, and reactive oxygen species (ROS) production regulation (4). In the context of SCI, mitochondrial dysfunction contributes significantly to secondary pathological alterations and neuronal death. Research on SCI models increasingly emphasizes mitochondrial impairment as a central factor affecting cellular metabolism, immune responses, axonal regeneration, and the renewal and differentiation of neural stem cells (5, 6). Ferroptosis, an iron-dependent form of regulated cell death, is triggered by the leakage of red blood cells, heme, and iron into injured tissues, leading to the generation of free radicals and subsequent toxicity (7). Ferroptosis plays a substantial role in SCI pathogenesis, with its acute phase occurring within 2 days and the subacute phase extending from 3 to 14 days post-injury (8). Furthermore, ferroptosis contributes to oxidative damage in neuronal cells following SCI by disrupting the redox balance (9). As primary ROS producers, mitochondria generate reactive species that accumulate, driving ferroptosis (10). Iron imbalance further aggravates mitochondrial dysfunction, impairing energy metabolism and increasing disease susceptibility (11). Beyond its role in iron uptake, storage, and utilization, mitochondrial iron overload aggravates dysfunction and ROS production, thereby promoting ferroptosis. However, the specific contributions of mitochondrial and ferroptosis-related genes in SCI pathogenesis remain incompletely understood. Further investigation into the interactions between mitochondria, ferroptosis, and SCI may yield insights for developing targeted therapeutic strategies, including novel drugs and treatment approaches for SCI.

This study identified mitochondrial and ferroptosis-related biomarkers through bioinformatics analysis of SCI-associated data from public databases. qPCR validation was performed on spinal cord samples from a rat SCI model collected on the second (acute phase) and seventh (subacute phase) days post-surgery, corresponding to the sample types in the database validation set. Additionally, molecular mechanisms of these biomarkers were examined using enrichment analysis, immune infiltration analysis, and regulatory network analysis, offering novel perspectives on SCI clinical treatment.

Materials and methods

Animal modeling

In SCI experimental models, urinary dysfunction is a common complication in animals. Female rats are typically selected for SCI studies owing to their relatively short and straight urethra, which simplifies postoperative management and minimizes the likelihood of urinary tract infections. For this study, 18 female SPF-grade SD rats, aged 8 weeks and weighing approximately 220 ± 20 grams, were sourced from Zhuhai Baishitong Biotechnology Co., Ltd. The animals were housed under standardized conditions, including controlled temperature, humidity, and a consistent light–dark cycle, with unrestricted access to food and water.

The rats were randomly assigned to three experimental groups: a sham surgery group ($n = 6$), a 2-day post-SCI group ($n = 6$), and a 7-day post-SCI group ($n = 6$). A SCI impact model was established to replicate human SCI. All procedures were performed at the Experimental Animal Research Center of Zhujiang Hospital, Southern Medical University (license number: SYXK (Guangdong) 2023-0215). The study received approval from the Ethics Committee of Zhujiang Hospital, Southern Medical University (approval number: LAEC-2024-120; approval date: June 21, 2024). Establishing the SCI model is a fundamental step in neuroscience research. In this study, a precise spinal cord impact device was employed to induce SCI in rats. Following anesthesia with isoflurane to ensure pain relief and unconsciousness, the rats were positioned prone, and the dorsal hair was shaved to prepare the area for surgery.

The surgical procedure involved a midline incision approximately 1.5 cm in length on the back. Using bony landmarks for guidance, the paraspinous muscles were dissected bluntly to fully expose the T10 vertebral lamina. A laminectomy was subsequently performed at the T10 level to facilitate the creation of the SCI model.

The study employed the 68099II spinal cord precision impactor from Shenzhen Ruiwoerd Life Science and Technology Co., Ltd., which offers precise control over impact speed, depth, and dwell time, ensuring accurate SCI induction. The impactor settings included a size 2 impact head, an impact velocity of 2 m/s, a depth of 1.2 mm, and a dwell time of 0.5 s. This controlled impact generated a significant hematoma at the targeted spinal segment.

Following SCI, the hematoma underwent dynamic changes over time. During the hyperacute phase, bleeding and inflammation exacerbated the hematoma, which gradually resolved in the later stages. This progression was typical of the natural course after SCI. The contusion also induced temporary involuntary spasms in the hind limbs and tail rigidity, serving as indicators of a successfully established and standardized SCI model.

Postoperatively, the muscles and skin were sutured in layers. To support the animals' physiological function, manual bladder expression was performed three times daily for 1 week following the injury to ensure adequate urine elimination. In the sham group, rats underwent a laminectomy at the T10 level, preserving the spinal cord and maintaining normal BBB (Basso, Beattie, and Bresnahan) locomotor scores postoperatively.

At 2 and 7 days post-SCI, animals were anesthetized with a 40 mg/kg intraperitoneal injection of 1% pentobarbital sodium. Following cardiac perfusion with phosphate-buffered saline, spinal cord samples were harvested for subsequent qPCR analysis.

Data acquisition

The gene expression omnibus (GEO) database¹ provided SCI-associated microarray expression profiles, specifically GSE109902 and GSE166009. The GSE109902 dataset, derived from the GPL22396 platform, included 20 spinal cord tissue samples from SCI rats and 10 from control rats. The GSE166009 dataset, based on the GPL27597 platform, contained 12 spinal cord tissue samples, consisting of nine from SCI rats and three from controls. Additionally, 1,136 mitochondria-related human genes were obtained from the MitoCarta 3.0 database² and subsequently mapped to rat homologs, resulting in 1,119 rat homologous genes (MRGs) (Supplementary Table S1). A total of 431 ferroptosis-related human genes retrieved from the literature were similarly converted to their rat homologs, yielding 437 rat genes (FRGs) (Supplementary Table S2) (12).

Weighted gene co-expression network analysis

Expression data of MRGs and FRGs from the GSE109902 dataset were used to calculate single-sample gene set enrichment analysis (ssGSEA) scores via the GSVA package (v 1.42.0) (13). The Wilcoxon test was then applied to compare MRG and FRG scores between SCI and control groups ($p < 0.05$). A co-expression network was constructed using MRG and FRG scores as traits within the GSE109902 dataset through the weighted gene co-expression network analysis (WGCNA) package (v 1.7.1) (14). Outlier samples were first removed using hierarchical clustering based on Euclidean distance. The scale-free network evaluation coefficient (R^2) and mean connectivity were subsequently used to determine the optimal soft-threshold power (β). Genes exhibiting similar expression patterns were grouped into the same module using the hybrid dynamic tree cutting algorithm, with parameters set as $\text{minModuleSize} = 20$, $\text{deepSplit} = 2$, and $\text{mergeCutHeight} = 0.15$. Different colors were assigned to modules for visualization. A heatmap of trait-module correlations was generated, emphasizing modules significantly associated with both MRG and FRG scores ($|\text{cor}| > 0.3$ and $p < 0.05$). Genes within these modules were identified as key module genes, strongly correlated with MRG and FRG scores.

Differential expression analysis and functional enrichment

Differentially expressed genes (DEGs) between SCI and control samples in the GSE109902 dataset were identified using the DESeq2 package (1.34.0) (15), with thresholds set at $|\log_2 \text{Fold Change (FC)}| > 0.5$ and $p < 0.05$. A comprehensive visualization of DEG distribution was achieved by generating a volcano plot and heat map through the ggplot2 package (v 3.4.1) (16) and ComplexHeatmap-package (v 2.14.0) (17). A Venn diagram, constructed with the VennDiagram package (v 1.7.1) (18) was used to identify overlapping genes between key modular genes and DEGs, which were then classified as candidate genes.

These candidate genes were subjected to Gene Ontology (GO) annotation and Kyoto Encyclopedia of Genes and Genomes (KEGG) pathway enrichment analysis via the clusterProfiler package (v 4.2.2) (19), with pathways exhibiting $p < 0.05$ considered statistically significant. The co-expression network of candidate genes was constructed by mapping the genes onto GeneMANIA.³

Machine learning algorithms and tissue-specific analysis

Two machine learning algorithms, least absolute shrinkage and selection operator (LASSO) and Boruta, were applied to identify feature genes associated with SCI from the candidate genes in the GSE109902 dataset. For LASSO analysis, the glmnet package (v 4.1–4) (20) was employed, with a lambda value of 0 selected as optimal for feature gene selection. Boruta analysis was performed using the Boruta package (v 8.0.0) (21) with default parameters. Subsequently, the common feature genes identified by both algorithms were determined through overlapping the results using the VennDiagram package (v 1.7.1).

Expression trends of the common feature genes were further compared between SCI and control samples in the GSE109902 and GSE166009 datasets using the Wilcoxon test. Emphasis was placed on genes exhibiting stable expression, defined as those with consistent expression patterns across both datasets and significant differential expression between groups ($p < 0.05$), which were selected as biomarkers for this study.

To assess tissue specificity, gene expression levels were analyzed using the online tool genotype-tissue expression (GTEx, <https://gtexportal.org/home/>).

Construction of artificial neural network

An artificial neural network (ANN) diagnostic model was developed to predict SCI likelihood based on the expression levels of identified biomarkers. After normalizing data from the GSE109902 dataset, the model was constructed using the neuralnet package (v 1.44.2) (22), employing the min-max method and configuring three hidden layers. To evaluate the model's predictive accuracy, the receiver operating characteristic (ROC) curve was generated using the pROC package (v 1.18.0) (23). An area under the curve (AUC) exceeding 0.7 was considered indicative of high accuracy.

Enrichment analysis of biomarkers

To elucidate the signaling pathways related to the biomarkers, GSEA was conducted on the GSE109902 dataset. Initially, Spearman correlation analysis was performed between the biomarkers and other genes across all samples using the psych package (v 2.1.6). Genes were then ranked based on their correlation coefficients, from highest to lowest. Concurrently, GSEA was carried out using the clusterProfiler package (v 4.2.2), with the "c2.cp.kegg.v7.4.symbols.gmt" gene set from the Molecular Signatures Database (MSigDB, <http://www.>

1 <http://www.ncbi.nlm.nih.gov/geo/>

2 <http://www.broadinstitute.org/mitocarta>

3 <http://genemania.org/>

TABLE 1 Primers of RT-qPCR used in this study.

| Gene | Primers forward (5'–3') | Product size (bp) |
|-------|--------------------------------------|-------------------|
| HCRT | Forward: TTC TAC AAA GGT TCC CTG GG | 20 |
| | Reverse: AAC AGT TCG TAG AGA CCG C | 19 |
| CDCA2 | Forward: TCT CCA CAG TAA CCG TAG AG | 20 |
| | Reverse: GGG AAG ATG ATG ACT TTC CTG | 21 |
| GAPDH | Forward: ACT CTA CCC ACG GCA AGT TC | 20 |
| | Reverse: TGG GTT TCC CGT TGA TGA CC | 20 |

gsea-msigdb.org/gsea/msigdb/index.jsp) as the reference. The thresholds for statistical significance were set at adj. $p < 0.05$ and $|\text{Normalized Enrichment Score (NES)}| > 1$.

Additionally, the biomarkers were analyzed using the GeneMANIA database (see text footnote 3) to predict genes associated with the biomarkers' functions and the biological processes in which they participate.

Immune infiltration analysis

Immune cell infiltration plays a critical role in characterizing disease defense mechanisms, offering insights into the extent of immune involvement in specific pathologies. In this study, infiltration levels of 22 immune cell types were quantified in samples from the GSE109902 dataset using the CIBERSORT algorithm (24). Differential immune cell infiltration between SCI and control samples was then assessed via the Wilcoxon test ($p < 0.05$). Additionally, Spearman correlation coefficients were calculated to examine the relationships between the immune cell types, as well as between biomarkers and immune cell infiltration, based on the expression matrix of biomarkers and immune cell levels.

Correlation analysis with inflammatory factors

The SCI process is typically associated with the release of inflammatory factors (25). To explore the relationship between biomarkers and inflammatory factors, 200 inflammation-related genes (IRGs) were retrieved from the MSigDB database using the search term "HALLMARK_INFLAMMATORY_RESPONSE." These 200 IRGs formed the background gene set for subsequent analysis. ssGSEA was then conducted on the GSE109902 dataset via the GSVA package to calculate the IRG score for each sample. Differences in IRG scores between the SCI and control groups were assessed ($p < 0.05$). Additionally, the relationship between biomarkers and IRGs was examined by calculating Spearman correlation coefficients and their significance, with the thresholds set at $|\text{cor}| > 0.3$ and $p < 0.05$.

Molecular regulatory network analysis

To investigate the regulatory factors targeting the biomarkers, upstream transcription factors (TFs) were identified through the

miRNet database.⁴ Additionally, microRNAs (miRNAs) regulating the biomarkers were detected using miRecords,⁵ miRTarBase,⁶ and TarBase.⁷ The upstream long non-coding RNAs (lncRNAs) of the identified miRNAs were further explored in the same databases to elucidate the molecular mechanisms governing the biomarkers. Finally, the TF-biomarker and lncRNA-miRNA-mRNA (biomarker) networks were visualized using Cytoscape software (v 3.10.1) (26) based on the predicted results.

Drug prediction and molecular docking

Potential drugs targeting biomarkers were identified through an in-depth analysis of the Enrichr database⁸ to support drug prediction and inform therapeutic strategies for SCI. The relationship between biomarkers and drugs was further examined by obtaining biomarker protein structures from the Protein Data Bank (PDB) database.⁹ Molecular docking was conducted using the Chemical and Biological Docking (CB-Dock) platform,¹⁰ focusing on interactions with binding energies below 5 kcal/mol, indicative of stronger biomarker-drug affinity. The docking results were subsequently visualized using PyMOL software (v 3.0.3) (27) to facilitate structural interpretation and analysis.

Real-time quantitative polymerase chain reaction

Spinal cord samples from T10 were collected at 2 and 7 days post-SCI, immediately frozen, and stored at -80°C (six samples per group). Total RNA was extracted using TRIzol reagent (Thermo Fisher Scientific, Inc.) and reverse transcribed into complementary DNA (cDNA). Thermal cycling was performed under the following conditions: denaturation at 95°C for 30 s, annealing at 95°C for 3 s, and extension at 60°C for 30 s. GAPDH mRNA served as the endogenous control, and results were quantified using the $2^{-\Delta\Delta CT}$ method. The primers utilized in this study were listed in Table 1. Since the experiment involved comparing data from postoperative day 2 and

4 <https://www.mirnet.ca/>

5 <https://ngdc.cncb.ac.cn/databasecommons/database/id/1310>

6 <https://ngdc.cncb.ac.cn/databasecommons/database/id/167>

7 <https://dianalab.e-ce.uth.gr/tarbasev9>

8 <https://maayanlab.cloud/Enrichr/>

9 <https://www.rcsb.org/>

10 <https://cadd.labshare.cn/cb-dock2/php/index.php>

postoperative day 7 with the control group, we selected one-way analysis of variance (one-way ANOVA) as the statistical analysis method.

Statistical analysis

Data processing and statistical analysis were conducted using R software (v 4.2.2). Group differences were assessed using the Wilcoxon test, with statistical significance set at $p < 0.05$.

Results

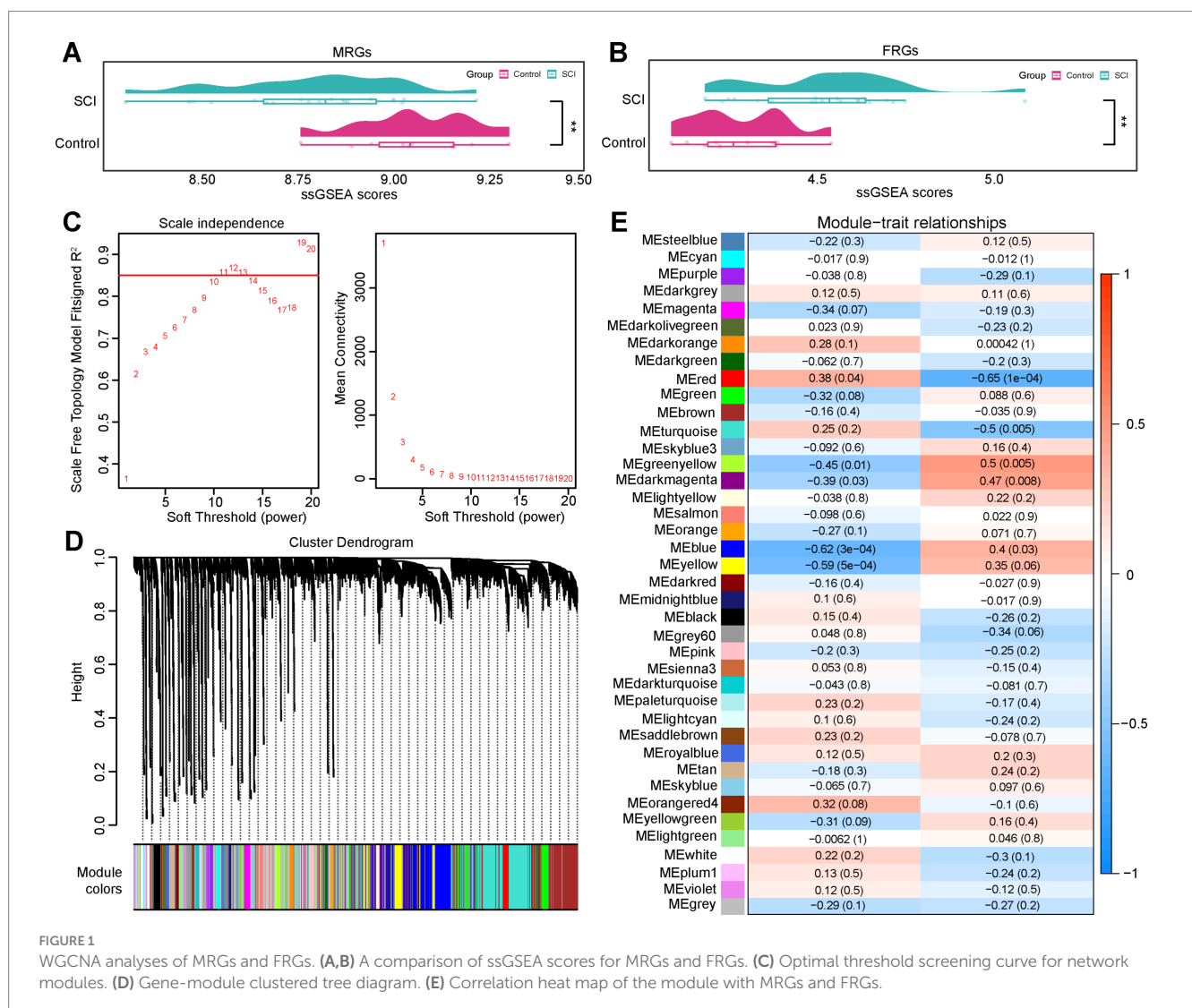
A total of 3,098 key module genes were obtained through WGCNA

The expression matrices of MRGs and FRGs in the GSE109902 dataset revealed significant differences in both the MRGs and FRGs scores between the SCI and control groups, with the SCI group exhibiting a lower MRGs score and a higher FRGs score ($p < 0.05$)

(Figures 1A,B), as determined by the ssGSEA algorithm. WGCNA was subsequently employed to identify gene clusters strongly associated with the MRGs and FRGs scores. Cluster analysis revealed no outlier samples. When the β -value was set to 11, the R^2 surpassed 0.85 (red line) and the mean connectivity approached zero, indicating optimal network consistency with a scale-free distribution and biological relevance (Figure 1C). Hierarchical clustering analysis identified 39 co-expression modules (excluding gray modules) (Figure 1D). Using a threshold of $|\text{cor}| > 0.3$ and $p < 0.05$, four modules—MEblue, MEdred, MEGreenyellow, and MEdarkmagenta—were found to be significantly correlated with the MRGs and FRGs scores (Figure 1E). In total, 3,098 genes within these modules were identified as key module genes associated with both the MRGs and FRGs scores.

Elucidation of biological functions associated with eight candidate genes

Using the criteria of $|\log_2\text{FC}| > 0.5$ and $p < 0.05$, 234 DEGs, consisting of 129 upregulated and 105 downregulated genes, were



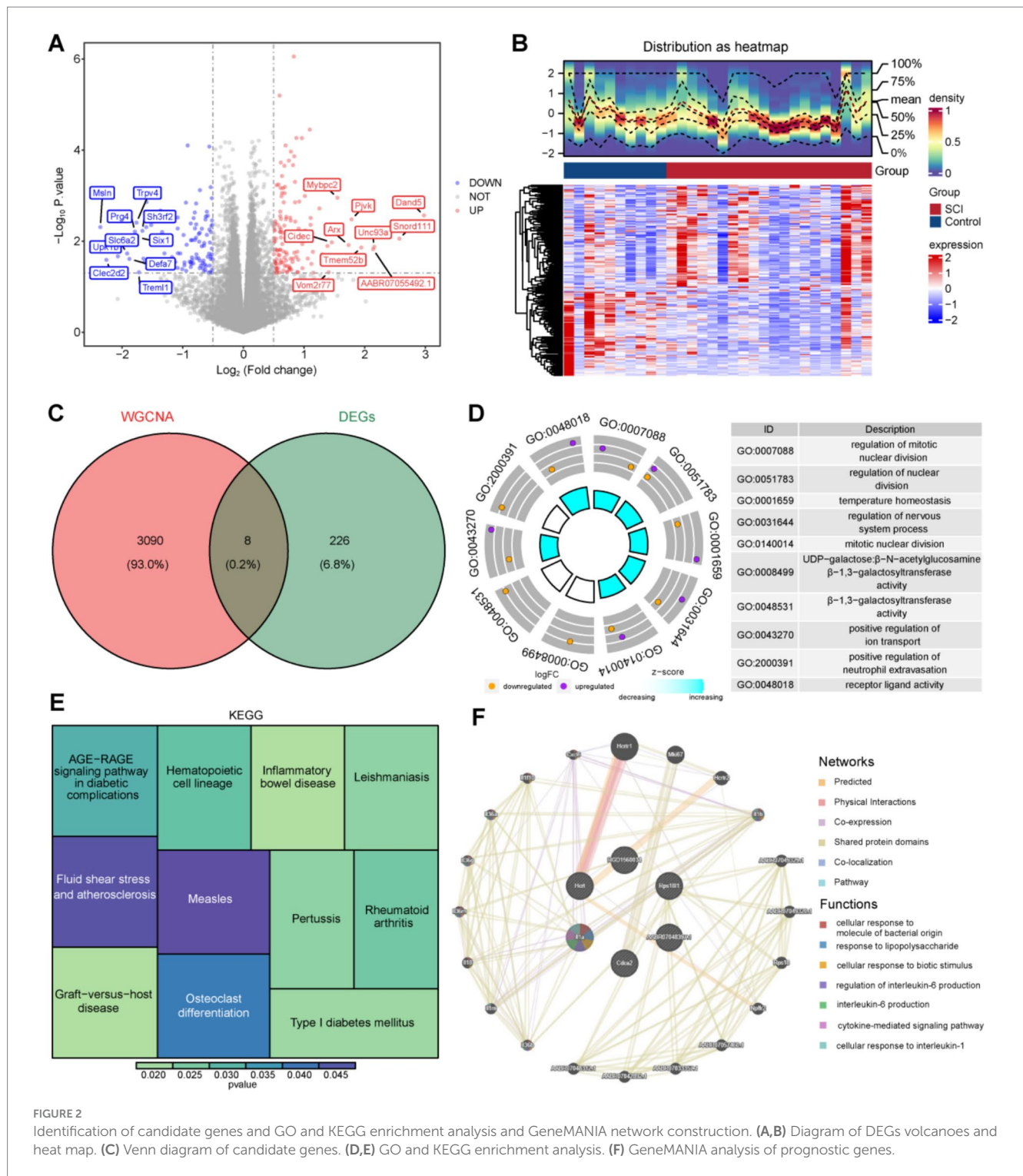


FIGURE 2

Identification of candidate genes and GO and KEGG enrichment analysis and GeneMANIA network construction. (A,B) Diagram of DEGs volcanoes and heat map. (C) Venn diagram of candidate genes. (D,E) GO and KEGG enrichment analysis. (F) GeneMANIA analysis of prognostic genes.

identified between SCI and control samples in GSE109902 (Figures 2A,B). Overlapping 3,098 key modular genes with the DEGs revealed eight mitochondrial and ferroptosis-associated genes, designated as candidate genes: U4, AABR07048397.1, Hcrt, Rps181l, Cdc2, SNORD115, RGD1560034, and Il1a (Figure 2C).

These candidate genes underwent enrichment analysis, resulting in 301 GO terms, including 280 biological processes (BPs), two cellular components (CCs), and 19 molecular functions (MFs), as well as 11 KEGG pathways ($p < 0.05$). The top 10 GO terms were

predominantly related to “regulation of mitotic nuclear division,” “regulation of nervous system processes,” “temperature homeostasis,” “positive regulation of ion transport,” and “positive regulation of neutrophil extravasation,” among others (Figure 2D). KEGG analysis highlighted the involvement of candidate genes in “inflammatory bowel disease,” “graft-versus-host disease,” and “osteoclast differentiation,” among other pathways (Figure 2E).

Furthermore, a GeneMANIA database search identified 20 functionally similar genes (e.g., Hcrt1, Mki67, Her2), and a

co-expression network was constructed to elucidate their roles in various processes, including “regulation of interleukin 6 production,” “interleukin 6 production,” and “cytokine-mediated signaling pathways” (Figure 2F).

Hcrt and Cdca2 were determined to be biomarkers in SCI

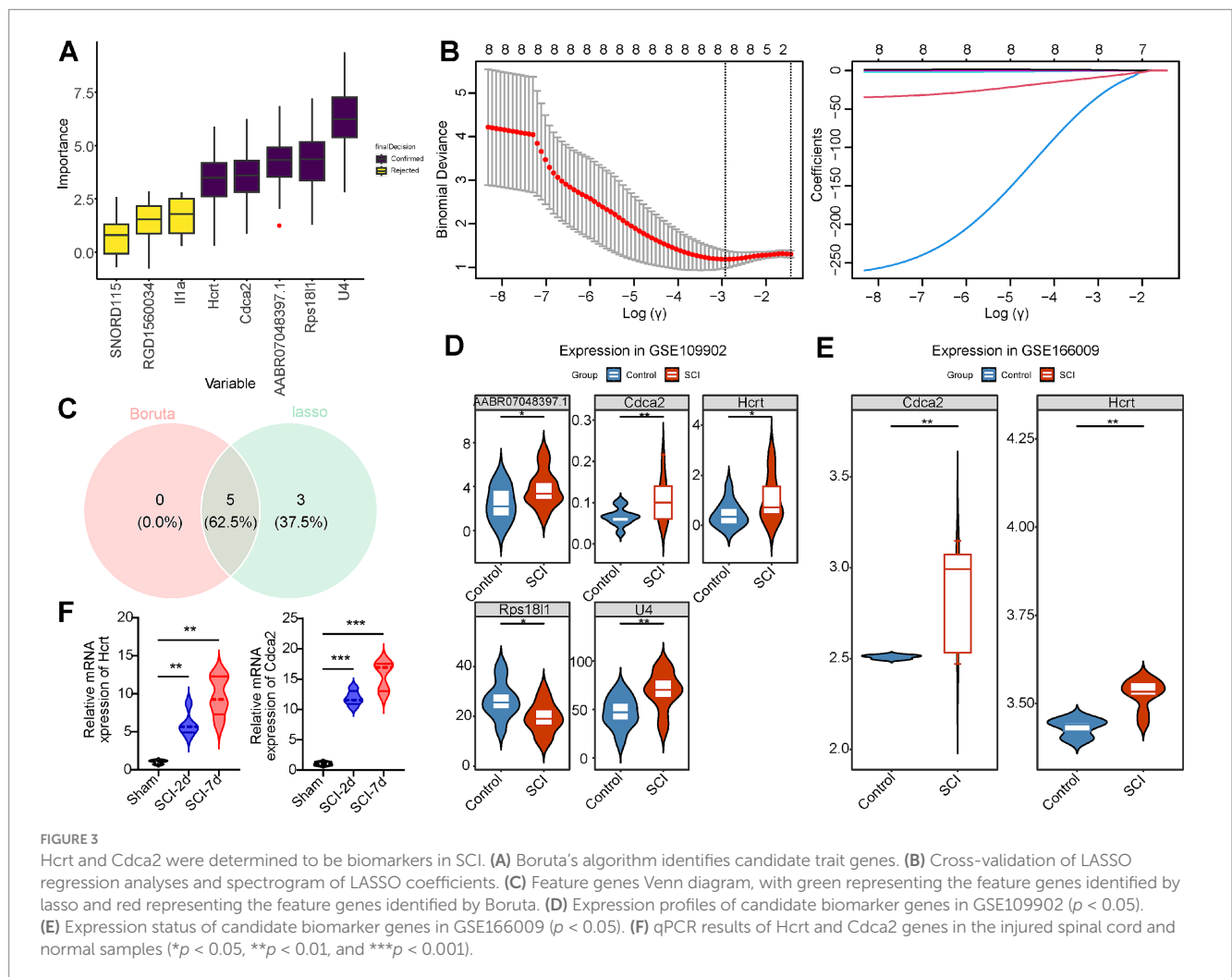
Two machine learning algorithms were employed to identify the most significant feature genes associated with SCI from the eight candidate genes. The Boruta algorithm highlighted five key genes (U4, AABR07048397.1, Hcrt, Rps181l, Cdca2) based on feature importance (Figure 3A). In LASSO analysis, conducted at a λ_{\min} value of 0.05360385, eight feature genes were selected: U4, AABR07048397.1, SNORD115, RGD1560034, Hcrt, Rps181l, Il1a, and Cdca2 (Figure 3B). An overlap analysis between the two algorithms revealed five common feature genes: U4, AABR07048397.1, Hcrt, Rps181l, and Cdca2 (Figure 3C).

The expression level analysis revealed significant differences in the five genes between the SCI and control groups in the GSE109902 dataset ($p < 0.05$) (Figure 3D). Similarly, Hcrt and Cdca2 exhibited significant differential expression between groups in the GSE166009 dataset ($p < 0.05$) (Figure 3E). qPCR validation was performed on rat spinal cord tissue samples collected at days

2 and 7 post-SCI surgery, showing a marked increase in the expression of both Hcrt and Cdca2 following the procedure. These results align with the expression patterns observed in the GSE166009 validation dataset, confirming the reliability of the screening process (Figure 3F). Notably, both Hcrt and Cdca2 demonstrated elevated expression in SCI samples compared to control samples across the two datasets. However, no expression of U4, AABR07048397.1, or Rps181l was detected in the GSE166009 dataset. Consequently, Hcrt and Cdca2 were selected as biomarkers for subsequent analyses.

Biomarkers specifically expressed in brain–spinal cord

The GTEx database was utilized to assess the expression levels of the two biomarkers across various tissues under physiological conditions. Hcrt exhibited higher expression in the brain, particularly in regions such as the hypothalamus, nucleus accumbens, frontal cortex, amygdala, and spinal cord (Figure 4A). In contrast, Cdca2 was predominantly expressed in tissues like the testis, EBV-transformed lymphocytes, cultured fibroblasts, and esophageal mucosa (Figure 4B). Notably, Cdca2 was also detectable in the brain, with the highest expression observed in the spinal cord.



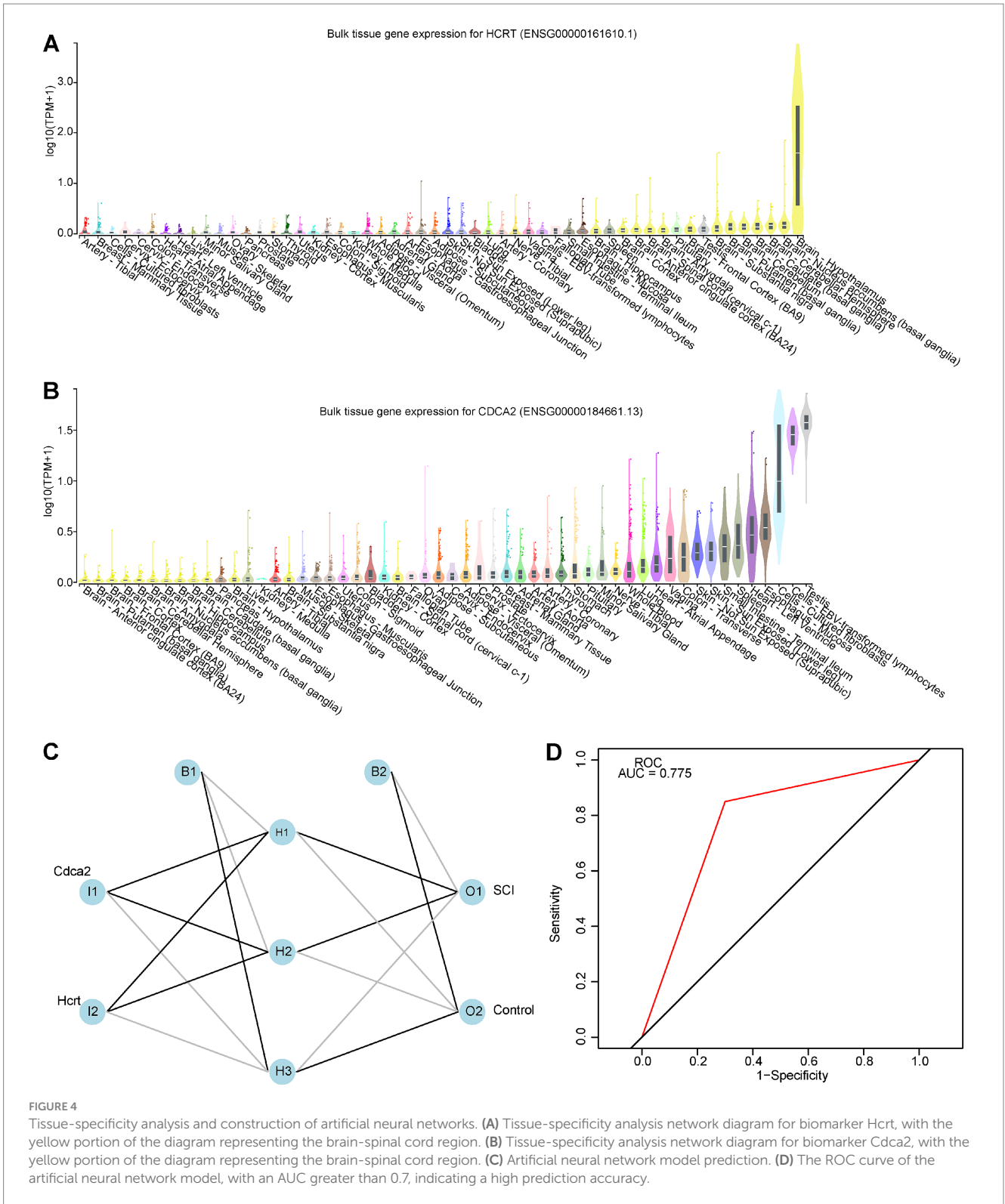


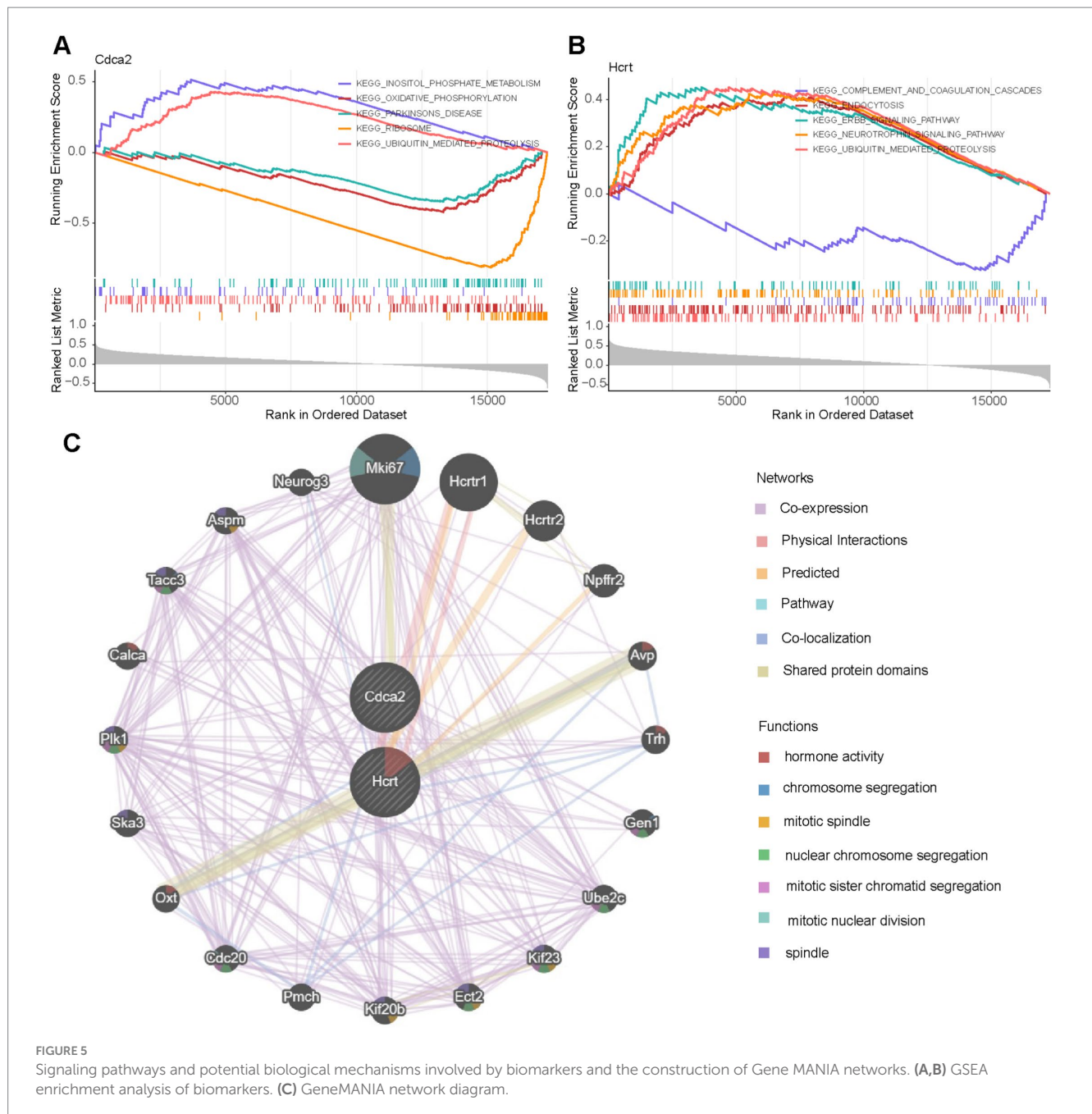
FIGURE 4 Tissue-specificity analysis and construction of artificial neural networks. **(A)** Tissue-specificity analysis network diagram for biomarker Hcrt, with the yellow portion of the diagram representing the brain-spinal cord region. **(B)** Tissue-specificity analysis network diagram for biomarker Cdca2, with the yellow portion of the diagram representing the brain-spinal cord region. **(C)** Artificial neural network model prediction. **(D)** The ROC curve of the artificial neural network model, with an AUC greater than 0.7, indicating a high prediction accuracy.

Building an effective artificial neural network for diagnosing SCI

An ANN model was developed using the GSE109902 dataset to improve differentiation between SCI and control samples by integrating the expression of two biomarkers (Figure 4C). The ROC curve yielded an AUC value of 0.775, suggesting that the ANN model exhibited robust accuracy in predicting SCI (Figure 4D).

Elucidating the biological mechanisms of biomarkers

The potential biological mechanisms of the biomarkers were analyzed using GSEA, identifying 19 enriched pathways for Hcrt and 16 for Cdca2 (adj. $p < 0.05$ and $|\text{NES}| > 1$). Shared enriched pathways included “ubiquitin-mediated proteolysis,” “endocytosis,” and the “neurotrophin signaling pathway” (Supplementary Tables S3, S4).



Cdca2 was also associated with pathways such as “oxidative phosphorylation,” “cytokine-cytokine receptor interaction,” “inositol phosphate metabolism,” and “sphingolipid metabolism” (Figure 5A). *Hcrt* expression showed significant correlations with the “ErbB signaling pathway,” “insulin signaling pathway,” “mTOR signaling pathway,” and “primary immunodeficiency,” among others. The top five pathways for each biomarker were visualized according to pathway significance (Figure 5B).

Additionally, co-expressed gene networks for the biomarkers were constructed using the GeneMANIA platform, comprising 39.02% co-expression, 25.61% physical interactions, 21.99% predicted interactions, 8.15% pathways, 2.86% co-localization, and 2.37% shared protein domains (Figure 5C). Both biomarkers were linked to 20 functionally related genes (e.g., *Mki67*, *Hcrt1*,

Hcrt2), participating in biological processes such as “hormone activity,” “chromosome segregation,” and “mitotic spindle” organization.

Biomarkers were linked to immune infiltrating cells in SCI

The infiltration levels of 22 immune cell types in each sample from the GSE109902 dataset were calculated using the CIBERSORT algorithm, as illustrated in Figure 6A. The Wilcoxon test revealed significant differences in T follicular helper cell levels between SCI and control samples, with lower levels observed in SCI samples ($p < 0.05$) (Figure 6B). Correlation analysis indicated that T follicular helper cells

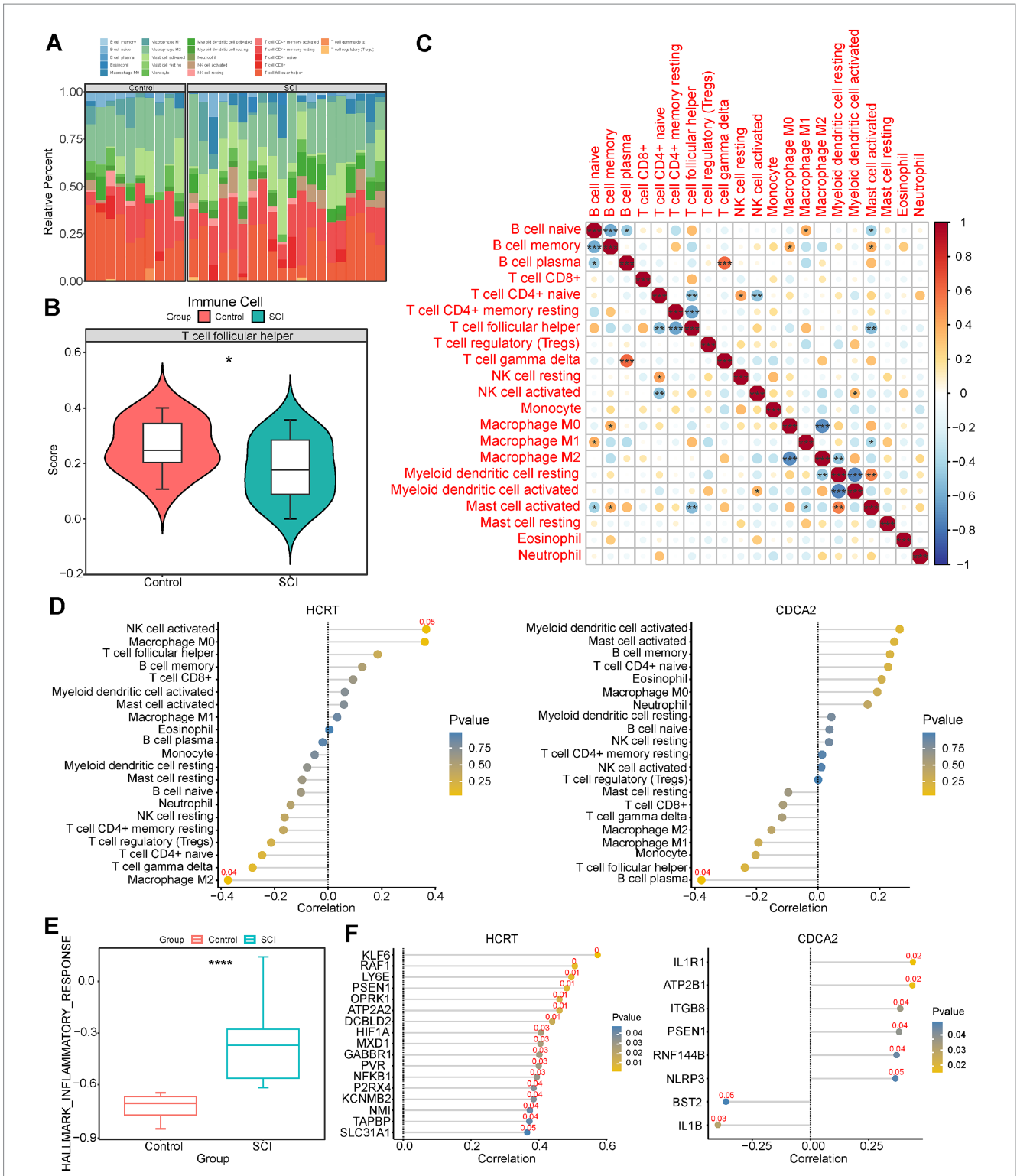


FIGURE 6 Immune infiltration analysis of biomarkers and analysis of correlation with inflammatory factors. **(A)** Immune cell infiltration between SCI and control groups. **(B)** Differences in immune cells between SCI and controls. **(C)** Correlation between immune cells. **(D)** Correlation between biomarkers and immune cells. **(E)** ssGSEA scores of inflammation-related genes in SCI samples and normal samples. **(F)** Correlation between biomarker and immune cells.

were negatively associated with naive CD4⁺ T cells ($cor = -0.51$, $p = 0.004$), activated mast cells ($cor = -0.53$, $p = 0.003$), and resting memory CD4⁺ T cells ($cor = -0.63$, $p < 0.001$) (Figure 6C).

Biomarker-immune cell correlation analysis further demonstrated a positive association between T follicular helper cells and Hcrt, alongside a negative association with Cdca2 (Figure 6D).

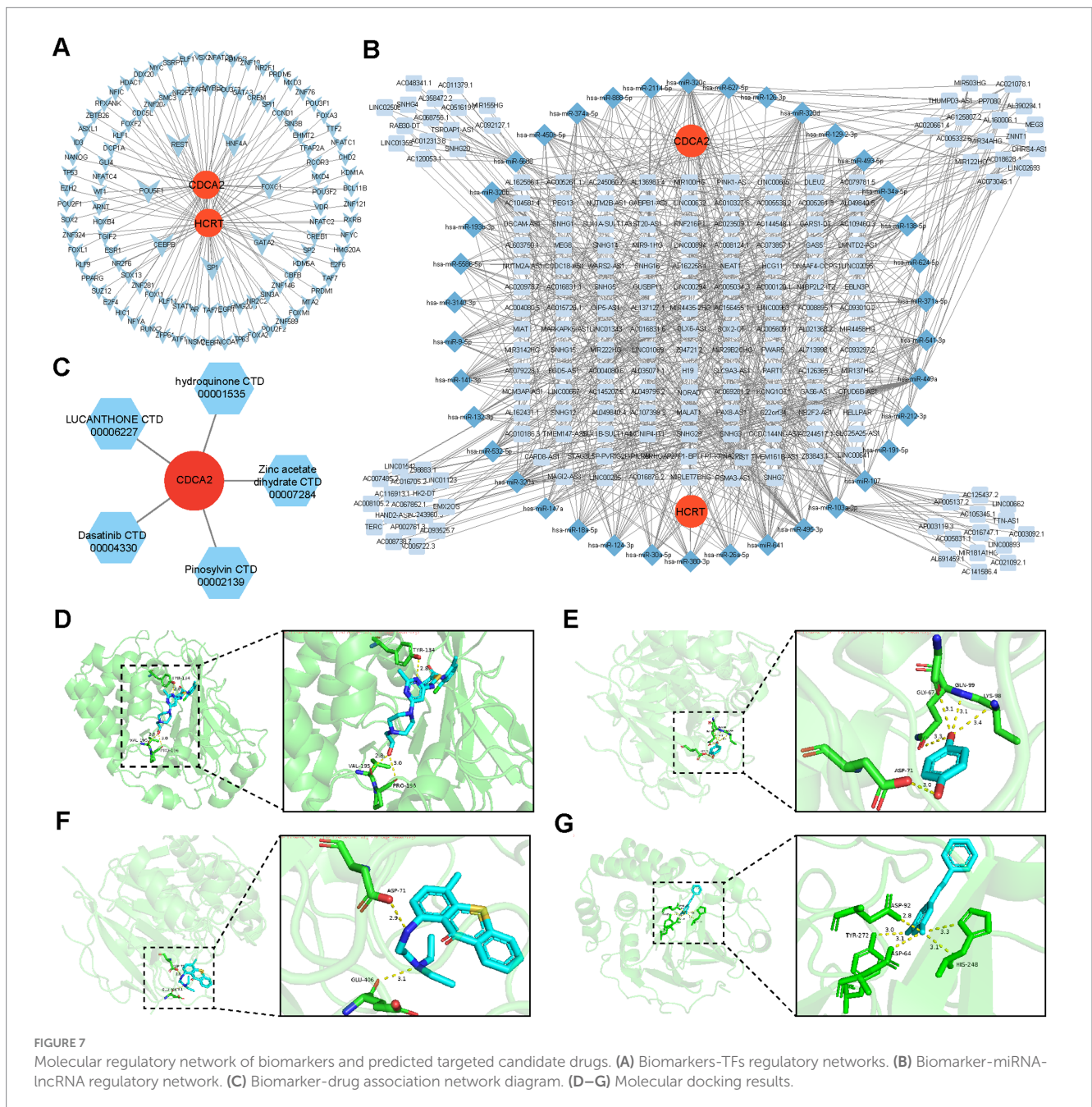
Biomarkers were linked to inflammatory factors in SCI

The inflammatory response plays a key role in the pathophysiology of SCI, with immune factors critically influencing its development and progression. The relationship between two specific biomarkers and 200 IRGs was assessed. Analysis using the ssGSEA algorithm revealed a significant difference in IRG scores between SCI and control samples in the GSE109902 dataset ($p < 0.05$), with higher scores detected in the SCI samples (Figure 6E). Correlation analysis showed that Hcrt exhibited significant positive correlations with 10 IRGs (e.g., KLF6, RAF1, LY6E), while Cdca2 demonstrated significant positive correlations with six IRGs (e.g., IL1R1, ATP2B1, PSEN1) and significant negative correlations with two IRGs (BST2 and IL1B) ($|cor$

>0.3 , $p < 0.05$) (Figure 6F). Notably, both Hcrt and Cdca2 were strongly positively correlated with PSEN1.

Potential regulatory mechanisms of biomarkers

Analysis of the miRNet database identified 110 TFs regulating the biomarkers, among which seven TFs (CEBPB, FOXC1, GATA2, HNF4A, REST, and SP1) were recognized as co-regulators of Hcrt and Cdca2 within the TF-biomarker network (Figure 7A). Additionally, predictions from individual databases identified 54 miRNAs targeting the biomarkers and 533 lncRNAs targeting these miRNAs. Within the lncRNAs-miRNAs-mRNAs network, numerous interaction pairs were



observed (Figure 7B). For instance, lncRNAs such as MALAT1, NEAT1, and XIST were predicted to regulate Hcrt expression via hsa-miR-30a-5p, while MALAT1 and XIST were also linked to the regulation of Cdca2 expression through miRNAs like hsa-miR-124-3p and hsa-miR-132-3p. These interactions suggest potential therapeutic targets for SCI.

Profiling drugs associated with biomarkers

Drug prediction via the Enrichr database identified five potential candidates associated with Cdca2: pinosylvin, zinc acetate dihydrate, hydroquinone, lucanthone, and dasatinib (Figure 7C). Notably, no drugs were predicted to interact with Hcrt. Molecular docking analysis demonstrated that all four drugs exhibited binding energies to Cdca2 below -5 kcal/mol (Table 2), suggesting stable interactions. The docking patterns of these four drugs with Cdca2 were subsequently visualized (Figures 7D–G).

Discussion

SCI represents a severe neurological and pathological condition characterized by extensive motor, sensory, and autonomic impairments (1). Progress in its treatment remains constrained due to the complex interplay of its temporospatial pathological mechanisms, which are intricately connected and challenging to define with precision. The limited capacity for neural regeneration continues to present significant hurdles, with no effective strategies yet available to overcome this bottleneck (28). Secondary injuries following SCI are closely associated with mitochondrial dysfunction and ROS production (29). Ferroptosis, an iron-dependent cell death mechanism marked by lipid peroxidation and disruptions in iron metabolism, is critically influenced by mitochondrial ROS, which promote lipid peroxidation and may trigger ferroptosis (30). Despite these insights, the molecular mechanisms underlying mitochondrial dysfunction and ferroptosis in SCI remain poorly understood. To address this, the study identified two biomarkers, Hcrt and Cdca2, linked to mitochondrial dysfunction and ferroptosis, through transcriptomic analysis of SCI models combined with bioinformatics approaches. Additional analyses, including GSEA, immune infiltration, and drug prediction, were performed. These results offer valuable insights into the pathogenesis of SCI and provide a foundation for developing innovative therapeutic strategies to improve patient outcomes.

The Hcrt gene encodes orexin, also known as hypocretin, first identified in 1998 by Lecea at the Scripps Research Institute and Sakurai at Southwestern Medical Center in Texas cloned the gene expressed in the lateral hypothalamus of rats, identifying a neuropeptide structurally similar to secretin and naming it hypocretin (31). Neuropeptides, a class of peptides synthesized by neurons and neuroendocrine cells in the central nervous system, bind to specific surface receptors to regulate neuronal activity. Their role in SCI primarily involves influencing neuronal function and survival. In the context of SCI, neuropeptides modulate neuronal excitability, synaptic plasticity, and synchronized neural activity, thereby impacting functional recovery (32). Hcrt is hypothesized to regulate SCI recovery by modulating neuropeptide signaling pathways, offering novel perspectives and potential therapeutic strategies for SCI treatment.

Cdca2 functions as a regulatory factor in cell cycle progression and acts as a subunit of phosphatase 1 γ (PP1 γ), contributing to critical cellular processes such as chromosome segregation, nuclear envelope reconstruction, microtubule organization, and DNA damage repair (33). In the context of SCI, cell cycle regulation significantly influences post-injury repair and regeneration. Alterations in the cell cycle after SCI are closely associated with neuronal survival, regeneration, and glial cell responses (34). Neuronal regenerative capacity is inherently limited after SCI, largely because mature neurons typically remain in the G0 phase, restricting their ability to re-enter the cell cycle for division and repair. Additionally, glial scar formation, a major barrier to axonal regeneration, is linked to glial cell proliferation and cell cycle regulation (35). Further investigation is required to clarify the specific role of Cdca2 in modulating cell cycle dynamics following SCI. CDCA2 can activate the BRCA1-NRF2 signaling pathway (36). This cascade reaction enhances cellular antioxidant capacity and effectively reduces the content of reactive oxygen species, thus highlighting the complex role of CDCA2 in regulating cellular redox homeostasis. Its mechanism is not only reflected in direct participation in the production and removal of ROS but also in the activation of downstream antioxidant signaling pathways, thereby maintaining intracellular redox balance and potentially influencing mitochondrial function and ferroptosis processes, ultimately impacting SCI. To date, no research has been published investigating the roles of Hcrt and Cdca2 in spinal cord injury. The next step involves validating these findings across various species to deepen our understanding of this critical area of study.

GSEA enrichment analysis identified significant enrichment of Hcrt in the neurotrophin and ErbB signaling pathways, while Cdca2 was prominently associated with the oxidative phosphorylation and

TABLE 2 The binding energy between biomarkers and active ingredients.

| Gene | Protein | PBD ID | Molecular name | Minimum binding free energy (kcal/mol) |
|-------|------------------------------------------|--------|----------------|----------------------------------------|
| CDCA2 | Cell division cycle-associated protein 2 | 5INB | Pinosylvin | -6.6 |
| CDCA2 | Cell division cycle-associated protein 2 | 5INB | Hydroquinone | -5.0 |
| CDCA2 | Cell division cycle-associated protein 2 | 5INB | Lucanthone | -6.6 |
| CDCA2 | Cell division cycle-associated protein 2 | 5INB | Dasatinib | -8.1 |

mTOR signaling pathways. The *Hcrt* gene, encoding orexin, is enriched in the ErbB signaling pathway, suggesting a potential role in the transformation of oligodendrocyte precursor cells and spontaneous remyelination following SCI, thereby contributing to its progression (37). The mTOR pathway, regulated by the mammalian target of rapamycin, is linked to the modulation of inflammation, apoptosis, and autophagy in SCI (38). Moreover, natural compounds derived from herbs and nutritional supplements may influence autophagy by targeting the mTOR pathway, presenting a potential therapeutic avenue in SCI management (39, 40). The association of *Cdca2* with the oxidative phosphorylation pathway suggests its involvement in SCI progression through the regulation of mitochondrial respiration and oxidative phosphorylation (41). This analysis establishes a basis for exploring the roles of *Hcrt* and *Cdca2* in SCI pathophysiology and highlights potential therapeutic interventions targeting these pathways.

The immunological analysis identified a significant reduction in T follicular helper cells (Tfh) in the SCI group compared to controls. SCI-induced immune deficiency syndrome (SCI-IDS), marked by systemic immunosuppression following SCI, substantially elevates the risk of infection and complicates therapeutic interventions. Research on the immune microenvironment emphasizes the role of Tfh cells in maintaining and refining immune system functionality. Evidence indicates that acute SCI downregulates CCR7 in peripheral tissues, reducing Tfh cell levels via chemokine signaling pathways, thereby contributing to SCI-IDS and worsening acute SCI (42). These results imply that *Hcrt* may influence immune responses through Tfh cells, thereby impacting SCI progression. Correlation analysis with inflammatory factors identified significant associations between the biomarkers and the inflammatory gene *PSEN1*. Mutations in *PSEN1* have been implicated in atypical Alzheimer's disease (AD) and non-AD phenotypes, including frontotemporal lobar degeneration (FTD), Parkinson's disease (PD), dementia with Lewy bodies (DLB), and spastic paraplegia (SP) (43). *PSEN1*, a component of the γ -secretase complex, regulates APP cleavage and may also modulate processes such as Notch signaling, β -catenin processing, and calcium homeostasis (44). Further investigation is needed to clarify the role of *PSEN1* in SCI and its potential as a mediator in the onset and progression of the condition.

An mRNA-miRNA-lncRNA network was constructed, identifying 54 miRNAs (e.g., miR-126, miR-132, miR-124) as potential regulators of the biomarkers, implicating their involvement in the post-transcriptional regulation of gene expression associated with SCI. Among them, miR-126 has been shown to promote angiogenesis and inhibit vascular inflammation in endothelial cells by targeting genes such as *SPRED1*, *PIK3R2*, and *VCAM1*, highlighting its regulatory role in vascular repair and inflammation following SCI (45). Additionally, miR-124 not only activates macrophages but also promotes their polarization from the M1 to the M2 phenotype, sustaining the M2 phenotype through enhanced miR-124 expression. This positions miR-124 as a key modulator of microglia/macrophage activity in the central nervous system. Evidence indicates that miR-124-3p, interacting with neuron-derived exosomes, suppresses M1 microglia activation via the MYH9/PI3K/AKT/NF- κ B signaling pathway, contributing to improved functional recovery after SCI (46).

This study identified 533 lncRNAs, including *MALAT1*, *NEAT1*, and *XIST*. Evidence suggests that *MALAT1* interacts with *Nrf2* to suppress neuron apoptosis associated with SCI (47). Additionally, *NEAT1* silencing has been shown to mitigate spinal cord injury and

decrease cavity formation by upregulating miR-29b (48). Knockdown of *NEAT1* also significantly attenuated SCI-related inflammation via the miR-211-5p/MAPK1 axis. Furthermore, the analysis revealed that lncRNAs such as *MALAT1*, *NEAT1*, and *XIST* regulated *Hcrt* expression through hsa-miR-30a-5p, while *MALAT1* and *XIST* modulated *Cdca2* expression via miRNAs such as hsa-miR-124-3p and hsa-miR-132-3p. Experimental validation remains necessary to substantiate these results.

Analysis using the Enrichr database identified five potential drugs interacting with *Cdca2*: pinosylvin, zinc acetate dihydrate, hydroquinone, lutanthone, and dasatinib. Molecular docking was performed to evaluate these interactions, with dasatinib demonstrating the lowest binding energy to *Cdca2*, indicative of the strongest intermolecular interaction. Dasatinib, an oral second-generation tyrosine kinase inhibitor, is widely used for treating Philadelphia chromosome-positive (Ph⁺) chronic myeloid leukemia (CML) and Ph⁺ acute lymphoblastic leukemia (ALL) (49). Beyond its established applications, dasatinib has been reported to modulate the LPS-induced neuroinflammatory response in microglia and astrocytes by inhibiting the AKT/STAT3 signaling pathway (50). Additionally, recent studies suggest that combining dasatinib with quercetin reverses senescence in LPS-stimulated primary cultured astrocytes and decreases pro-inflammatory cytokine levels. This combination has shown efficacy in alleviating spinal cord neuroinflammation and reducing hypersensitivity in a rat model of chronic constriction injury of the sciatic nerve (51).

Modulation of immune cell activity, including microglia and astrocytes, by dasatinib may contribute to mitigating neuroinflammatory responses, a key factor in the pathological progression of SCI. As a potential anti-inflammatory agent, the therapeutic potential of dasatinib for SCI and its association with mitochondrial dysfunction and ferroptosis warrant further investigation. This study primarily examines the role of ferroptosis during the acute and subacute phases, specifically on the 2nd and 7th days post-SCI. Future investigations should prioritize comprehensive evaluation of the pharmacological efficacy and safety profiles of these agents in SCI management, with particular emphasis on establishing methodological frameworks to assess their clinical viability as potential therapeutic candidates.

This study identifies *Cdca2* and *Hcrt* as biomarkers linked to mitochondrial function and ferroptosis in SCI, utilizing transcriptomic data, machine learning algorithms, and qPCR validation. The expression patterns of these biomarkers align with the dataset results, with statistically significant differences, confirming their relevance in SCI pathology. These findings offer valuable reference points and potential therapeutic targets for SCI treatment. Notably, ferroptosis may initiate within the first 2 h post-SCI, highlighting the importance of investigating earlier time points to elucidate its induction mechanisms. Additionally, the differential sensitivity of neural cell types to ferroptosis and the expression patterns of DEGs within these cells remain unexplored. Further research should focus on cell-specific ferroptosis sensitivity and its implications to uncover the distinct contributions of various neural cell types in SCI progression.

Data availability statement

The datasets presented in this study can be found in online repositories. The names of the repository/repositories and accession number(s) can be found in the article/Supplementary material.

Ethics statement

The animal studies were approved by Laboratory Animal Ethics Committee of Zhujiang Hospital of Southern Medical University (LAEC-2024-120). The studies were conducted in accordance with the local legislation and institutional requirements. Written informed consent was obtained from the owners for the participation of their animals in this study.

Author contributions

JZ: Conceptualization, Data curation, Formal analysis, Funding acquisition, Investigation, Methodology, Writing – original draft, Writing – review & editing. SW: Conceptualization, Software, Supervision, Validation, Visualization, Writing – review & editing. YZ: Writing – review & editing, Resources, Visualization, Supervision. CZ: Project administration, Resources, Writing – review & editing.

Funding

The author(s) declare that financial support was received for the research, authorship, and/or publication of this article. The research was supported by the Guangzhou Science and Technology Project (Grant No: 2024B03J0407) (The sponsor is Chusong Zhou).

References

- Anjum A, Yazid MD, Fauzi Daud M, Idris J, Ng AMH, Selvi Naicker A, et al. Spinal cord injury: pathophysiology, multimolecular interactions, and underlying recovery mechanisms. *Int J Mol Sci.* (2020) 21:7533. doi: 10.3390/ijms21207533
- Selvaraj A, Shokur S, Campos DSE, Donati ARC, Almeida S, Yamauti SY, et al. Non-invasive, brain-controlled functional electrical stimulation for locomotion rehabilitation in individuals with paraplegia. *Sci Rep.* (2019) 9:6782. doi: 10.1038/s41598-019-43041-9
- Ahuja CS, Nori S, Tetreault L, Wilson J, Kwon B, Harrop J, et al. Traumatic spinal cord injury-repair and regeneration. *Neurosurgery.* (2017) 80:S9–S22. doi: 10.1093/neuros/nyw080
- Jiang M, Bai M, Lei J, Xie Y, Xu S, Jia Z, et al. Mitochondrial dysfunction and the AKI-to-CKD transition. *Am J Physiol Renal Physiol.* (2020) 319:F1105–16. doi: 10.1152/ajprenal.00285.2020
- Slater PG, Dominguez-Romero ME, Villarreal M, Eisner V, Larrain J. Mitochondrial function in spinal cord injury and regeneration. *Cell Mol Life Sci.* (2022) 79:239. doi: 10.1007/s00018-022-04261-x
- Stewart AN, McFarlane KE, Vekaria HJ, Bailey WM, Slone SA, Trantham LA, et al. Mitochondria exert age-divergent effects on recovery from spinal cord injury. *Exp Neurol.* (2021) 337:113597. doi: 10.1016/j.expneurol.2021.113597
- Li J, Cao F, Yin H-L, Huang Z-J, Lin Z-T, Mao N, et al. Ferroptosis: past, present and future. *Cell Death Dis.* (2020) 11:88. doi: 10.1038/s41419-020-2298-2
- Li J-Z, Fan B-Y, Sun T, Wang X-X, Li J-J, Zhang J-P, et al. Bioinformatics analysis of ferroptosis in spinal cord injury. *Neural Regen Res.* (2023) 18:626–33. doi: 10.4103/1673-5374.350209
- Ge M-H, Tian H, Mao L, Li D-Y, Lin J-Q, Hu H-S, et al. Zinc attenuates ferroptosis and promotes functional recovery in contusion spinal cord injury by activating Nrf2/GPX4 defense pathway. *CNS Neurosci Ther.* (2021) 27:1023–40. doi: 10.1111/cns.13657
- Dan Dunn J, Alvarez LA, Zhang X, Soldati T. Reactive oxygen species and mitochondria: a nexus of cellular homeostasis. *Redox Biol.* (2015) 6:472–85. doi: 10.1016/j.redox.2015.09.005
- Wang H, Liu C, Zhao Y, Gao G. Mitochondria regulation in ferroptosis. *Eur J Cell Biol.* (2020) 99:151058. doi: 10.1016/j.ejcb.2019.151058

Conflict of interest

The authors declare that the research was conducted in the absence of any commercial or financial relationships that could be construed as a potential conflict of interest.

Generative AI statement

The authors declare that no Gen AI was used in the creation of this manuscript.

Publisher's note

All claims expressed in this article are solely those of the authors and do not necessarily represent those of their affiliated organizations, or those of the publisher, the editors and the reviewers. Any product that may be evaluated in this article, or claim that may be made by its manufacturer, is not guaranteed or endorsed by the publisher.

Supplementary material

The Supplementary material for this article can be found online at: <https://www.frontiersin.org/articles/10.3389/fneur.2025.1526966/full#supplementary-material>

- Wu J, Cai H, Lei Z, Li C, Hu Y, Zhang T, et al. Expression pattern and diagnostic value of ferroptosis-related genes in acute myocardial infarction. *Front Cardiovasc Med.* (2022) 9:993592. doi: 10.3389/fcvm.2022.993592
- Hänzelmann S, Castelo R, Guinney J. GSEA: gene set variation analysis for microarray and RNA-seq data. *BMC Bioinformatics.* (2013) 14:7. doi: 10.1186/1471-2105-14-7
- Langfelder P, Horvath S. WGCNA: an R package for weighted correlation network analysis. *BMC Bioinformatics.* (2008) 9:559. doi: 10.1186/1471-2105-9-559
- Love MI, Huber W, Anders S. Moderated estimation of fold change and dispersion for RNA-seq data with DESeq2. *Genome Biol.* (2014) 15:550. doi: 10.1186/s13059-014-0550-8
- Gustavsson EK, Zhang D, Reynolds RH, Garcia-Ruiz S, Ryten M. ggtranscript: an R package for the visualization and interpretation of transcript isoforms using ggplot2. *Bioinformatics.* (2022) 38:3844–6. doi: 10.1093/bioinformatics/btac409
- Gu Z, Hübschmann D. Make interactive complex heatmaps in R. *Bioinformatics.* (2022) 38:1460–2. doi: 10.1093/bioinformatics/btab806
- Gao C-H, Yu G, Cai P. ggVennDiagram: an intuitive, easy-to-use, and highly customizable R package to generate Venn diagram. *Front Genet.* (2021) 12:706907. doi: 10.3389/fgene.2021.706907
- Yu G, Wang L-G, Han Y, He Q-Y. clusterProfiler: an R package for comparing biological themes among gene clusters. *OMICS.* (2012) 16:284–7. doi: 10.1089/omi.2011.0118
- Friedman J, Tibshirani R. Regularization paths for generalized linear models via coordinate descent. *J Stat Softw.* (2010) 33:1–22. doi: 10.18637/jss.v033.i01
- Wang X, Jiang G, Zong J, Lv D, Lu M, Qu X, et al. Revealing the novel ferroptosis-related therapeutic targets for diabetic foot ulcer based on the machine learning. *Front Genet.* (2022) 13:944425. doi: 10.3389/fgene.2022.944425
- You H, Dong M. Identification of immuno-inflammation-related biomarkers for acute myocardial infarction based on bioinformatics. *J Inflamm Res.* (2023) 16:3283–302. doi: 10.2147/JIR.S421196
- Robin X, Turck N, Hainard A, Tiberti N, Lisacek F, Sanchez J-C, et al. pROC: an open-source package for R and S⁺ to analyze and compare ROC curves. *BMC Bioinformatics.* (2011) 12:77. doi: 10.1186/1471-2105-12-77

24. Newman AM, Liu CL, Green MR, Gentles AJ, Feng W, Xu Y, et al. Robust enumeration of cell subsets from tissue expression profiles. *Nat Methods*. (2015) 12:453–7. doi: 10.1038/nmeth.3337
25. Liu X, Zhang Y, Wang Y, Qian T. Inflammatory response to spinal cord injury and its treatment. *World Neurosurg*. (2021) 155:19–31. doi: 10.1016/j.wneu.2021.07.148
26. Shannon P, Markiel A, Ozier O, Baliga NS, Wang JT, Ramage D, et al. Cytoscape: a software environment for integrated models of biomolecular interaction networks. *Genome Res*. (2003) 13:2498–504. doi: 10.1101/gr.1239303
27. Seeliger D, de Groot BL. Ligand docking and binding site analysis with PyMOL and Autodock/Vina. *J Comput Aided Mol Des*. (2010) 24:417–22. doi: 10.1007/s10822-010-9352-6
28. Hu X, Xu W, Ren Y, Wang Z, He X, Huang R, et al. Spinal cord injury: molecular mechanisms and therapeutic interventions. *Signal Transduct Target Ther*. (2023) 8:245. doi: 10.1038/s41392-023-01477-6
29. Yao S, Pang M, Wang Y, Wang X, Lin Y, Lv Y, et al. Mesenchymal stem cell attenuates spinal cord injury by inhibiting mitochondrial quality control-associated neuronal ferroptosis. *Redox Biol*. (2023) 67:102871. doi: 10.1016/j.redox.2023.102871
30. Bao J, Yang S. scRNA analysis and ferroptosis-related ceRNA regulatory network investigation in microglia cells at different time points after spinal cord injury. *J Orthop Surg Res*. (2023) 18:701. doi: 10.1186/s13018-023-04195-5
31. Jacobson LH, Hoyer D, de Lecea L. Hypocretins (orexins): the ultimate translational neuropeptides. *J Intern Med*. (2022) 291:533–56. doi: 10.1111/joim.13406
32. Zeng Y-S, Ding Y, Xu H-Y, Zeng X, Lai B-Q, Li G, et al. Electro-acupuncture and its combination with adult stem cell transplantation for spinal cord injury treatment: a summary of current laboratory findings and a review of literature. *CNS Neurosci Ther*. (2022) 28:635–47. doi: 10.1111/cns.13813
33. Lin X, Zou Z, Zhong J, Wang T, Ma W, Hu T, et al. The role of CDCA2 in tumor genesis, prognosis and future treatments. *Eur J Cancer*. (2024) 211:114308. doi: 10.1016/j.ejca.2024.114308
34. Milich LM, Ryan CB, Lee JK. The origin, fate, and contribution of macrophages to spinal cord injury pathology. *Acta Neuropathol*. (2019) 137:785–97. doi: 10.1007/s00401-019-01992-3
35. Wu J, Stoica BA, Faden AI. Cell cycle activation and spinal cord injury. *Neurotherapeutics*. (2011) 8:221–8. doi: 10.1007/s13311-011-0028-2
36. Wang S, Cao K, Liao Y, Zhang W, Zheng J, Li X, et al. CDCA2 protects against oxidative stress by promoting BRCA1-NRF2 signaling in hepatocellular carcinoma. *Oncogene*. (2021) 40:4368–83. doi: 10.1038/s41388-021-01855-w
37. Bartus K, Burnside ER, Galino J, James ND, Bennett DLH, Bradbury EJ. ErbB receptor signaling directly controls oligodendrocyte progenitor cell transformation and spontaneous remyelination after spinal cord injury. *Glia*. (2019) 67:1036–46. doi: 10.1002/glia.23586
38. Wang X, Fu Y, Botchway BOA, Zhang Y, Zhang Y, Jin T, et al. Quercetin can improve spinal cord injury by regulating the mTOR signaling pathway. *Front Neurol*. (2022) 13:905640. doi: 10.3389/fneur.2022.905640
39. Wu C, Chen H, Zhuang R, Zhang H, Wang Y, Hu X, et al. Betulinic acid inhibits pyroptosis in spinal cord injury by augmenting autophagy via the AMPK-mTOR-TFEB signaling pathway. *Int J Biol Sci*. (2021) 17:1138–52. doi: 10.7150/ijbs.57825
40. Du Y, Cai X. Therapeutic potential of natural compounds from herbs and nutraceuticals in spinal cord injury: regulation of the mTOR signaling pathway. *Biomed Pharmacother*. (2023) 163:114905. doi: 10.1016/j.biopha.2023.114905
41. Forston MD, Wei GZ, Chariker JH, Stephenson T, Andres K, Glover C, et al. Enhanced oxidative phosphorylation, re-organized intracellular signaling, and epigenetic de-silencing as revealed by oligodendrocyte transcriptome analysis after contusive spinal cord injury. *Sci Rep*. (2023) 13:21254. doi: 10.1038/s41598-023-48425-6
42. Li C, Wu C, Xu G, Liu Y, Chen J, Zhang J, et al. CCR7-mediated T follicular helper cell differentiation is associated with the pathogenesis and immune microenvironment of spinal cord injury-induced immune deficiency syndrome. *Front Neurosci*. (2022) 16:1019406. doi: 10.3389/fnins.2022.1019406
43. Yang Y, Bagyinszky E, An SSA. Presenilin-1 (PSEN1) mutations: clinical phenotypes beyond Alzheimer's disease. *Int J Mol Sci*. (2023) 24:8417. doi: 10.3390/ijms24098417
44. Bagaria J, Bagyinszky E, An SSA. Genetics, functions, and clinical impact of presenilin-1 (PSEN1) gene. *Int J Mol Sci*. (2022) 23:10970. doi: 10.3390/ijms231810970
45. Hu J, Zeng L, Huang J, Wang G, Lu H. miR-126 promotes angiogenesis and attenuates inflammation after contusion spinal cord injury in rats. *Brain Res*. (2015) 1608:191–202. doi: 10.1016/j.brainres.2015.02.036
46. Wang J, Tian F, Cao L, Du R, Tong J, Ding X, et al. Macrophage polarization in spinal cord injury repair and the possible role of microRNAs: a review. *Heliyon*. (2023) 9:e22914. doi: 10.1016/j.heliyon.2023.e22914
47. Hu J, Huang K, Bao F, Zhong S, Fan Q, Li W. Low-dose lipopolysaccharide inhibits spinal cord injury-induced neuronal apoptosis by regulating autophagy through the lncRNA MALAT1/Nrf2 axis. *PeerJ*. (2023) 11:e15919. doi: 10.7717/peerj.15919
48. Bai G, Jiang L, Meng P, Li J, Han C, Wang Y, et al. LncRNA Neat1 promotes regeneration after spinal cord injury by targeting miR-29b. *J Mol Neurosci*. (2021) 71:1174–84. doi: 10.1007/s12031-020-01740-3
49. Advani AS, Moseley A, O'Dwyer KM, Wood BL, Park J, Wieduwilt M, et al. Dasatinib/prednisone induction followed by blinatumomab/dasatinib in Ph⁺ acute lymphoblastic leukemia. *Blood Adv*. (2023) 7:1279–85. doi: 10.1182/bloodadvances.2022008216
50. Ryu K-Y, Lee H-J, Woo H, Kang R-J, Han K-M, Park H, et al. Dasatinib regulates LPS-induced microglial and astrocytic neuroinflammatory responses by inhibiting AKT/STAT3 signaling. *J Neuroinflamm*. (2019) 16:190. doi: 10.1186/s12974-019-1561-x
51. Du J, Cheng N, Deng Y, Xiang P, Liang J, Zhang Z, et al. Astrocyte senescence-like response related to peripheral nerve injury-induced neuropathic pain. *Cell Mol Biol Lett*. (2023) 28:65. doi: 10.1186/s11658-023-00474-5